Journal Name

COMMUNICATION

Pasteur's Tartaramide/Malamide Quasiracemates: New Entries and Departures from Near Inversion Symmetry

Received 00th January 20xx,
Accepted 00th January 20xx

DOI: 10.1039/x0xx00000x

www.rsc.org/

Emily. N. Pinter,[a] Lee S. Cantrell,[b] Graeme M. Day,[c] and Kraig A. Wheeler[b]

This investigation explores Pasteur's 1853 (+)-tartaramide/(-)-malamide quasiracemate, extends this system to the crystallization behavior of methyl and butyl derivatives, and challenges the well-known notion that pairs of quasienantiomers assemble without exception to give near centrosymmetric crystal packing motifs. Each of the structures included in this study exhibits an extensive set of N/O-H···O contacts with component alignment in the quasiracemates defined by inversion and/or glide symmetry. Solid-state functional density theory calculations were applied to quantify the crystal stabilization and rationalize the observed packing tendencies.

L. Pasteur's work on tartaric acid from the 1840's and 50's[1-4] continues to attract intense interest due to the striking simplicity of this building block[5], its use as a facile entry point to molecular asymmetry[6-8], and complex crystallization landscapes[9-11]. While Pasteur's discoveries are widely recognized as one of the earliest systematic investigations of optical activity and spontaneous resolution, less known is his work on the cocrystallization behaviour of tartaric acid and its derivatives with secondary coformers. One such entry is related to Pasteur's 1853 'combination compounds' derived from equal portions of ammonium (+)-bitartrate and ammonium (-)-bimalate (**1**).[1] This material represents one of the first known examples of a class of compound now commonly referred to as quasiracemates or quasiracemic materials, where the two building blocks mimic true racemates by a slight chemical modification to the chemical framework or pendant substituent of one of the components.[12]

Our recent investigation of Pasteur's quasiracemate **1** highlighted unusual heteroepitaxial crystal growth of the building blocks to produce three-component dumbbell shaped crystals.[9] Other literature reports also focus on the rich crystal architectures that arise from combining tartrate and malate quasienantiomers.[13-18] Two important themes emerge from these collective efforts. The first is that quasiracemate formation readily occurs despite the seemingly odd pairing of tartrate and malate. Unlike the majority of known quasiracemic systems that utilize structurally similar quasienantiomers, the success of cocrystallizing systems from tartrate and malate frameworks is rather unexpected because of the differences in sterics and electrostatic features associated with the change from an OH to an H substituent on such a small molecule. Secondly, in each instance combining the quasienantiomers leads to bimolecular crystalline assemblies that approximate inversion symmetry. Whether by coincidence or systematic study, the combined use of the tartrate/malate molecular structures offers an important pathway to these cocrystalline assemblies because they are presumably more energetically favorable than crystals consisting of only the enantiomerically pure starting materials. The energetic stabilization in observed cocrystals of small organic molecules is usually small (less than 10 kJ mol $^{-1}$ of molecules), sometimes ranging up to 20-30 kJ mol^{-1}.[19] In the case of quasiracemates, much of the driving force behind these assemblies relates to the shape complementarity of quasienantioimers and the efficient crystal packing achieved from the pairwise organization of these left and right handed molecular components.

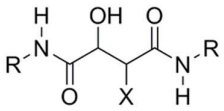

X = OH (**2**) or H (**3**)
R = H, Methyl, Butyl

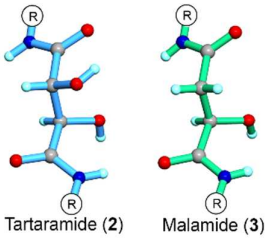

Tartaramide (**2**) Malamide (**3**)

[a] *Department of Chemistry, Indiana University, 800 East Kirkwood Avenue, Bloomington, IN, 47405, USA.*
[b] *Department of Chemistry, Whitworth University, 304 W Hawthorne Drive, Spokane, WA 99251, USA. Email: kraigwheeler@whitworth.edu*
[c] *Department of Chemistry, University of Southampton, University Road, Southampton, SO17 1BJ, UK. Email: G.M.Day@soton.ac.uk*

† Electronic Supplementary Information (ESI) available: Synthetic procedures, NMR spectroscopic data, full crystal structure and hydrogen bond tables, computational modelling, differential scanning calorimetry results. CCDC 1832191-1832198. For ESI and crystallographic data in CIF or other electronic format see DOI: 10.1039/x0xx00000x

Another interesting aspect of Pasteur's 1853 report is the identification of a second quasiracemic compound derived from the (+)-tartaramide, (+)-**2**-H, and (-)-malamide, (-)-**3**-H, components. Pasteur's studies of quasiracemates **1** and (+)-**2**-H/(-)-**3**-H are all the more remarkable considering that the material discovery process from the period, albeit often well-crafted and meticulous, utilized primitive assessment tools (*e.g.,* melting point behavior, solubility, and optical rotation) by today's standards to distinguish the various crystalline phases.

This contribution examines the structural preferences of quasiracemate (+)-**2**-H/(-)-**3**-H as well as two previously unreported methyl and butyl amide derivatives. In addition to offering new perspectives to these historically important materials, the family of crystal structures determined for this study challenge the well-known notion that pairs of quasienantiomers assemble without exception to give near centrosymmetric motifs. We complement the structural study with dispersion corrected density functional theory (DFT-D) calculations on both crystals and single molecules to understand the impact of the OH/H group variation to crystal stabilization of the quasiracemic systems and to rationalize the approximate symmetry present in the observed structures.

Crystal Structure Assessment

Tartaramide/Malamide. Several views of the crystal structures of quasiracemate (+)-**2**-H/(-)-**3**-H and the racemic counterparts [(±)-**2**-H, (±)-**3**-H] are shown in Fig. 1. Though racemic tartaramide (±)-**2**-H ($P2_1/c$) and quasiracemate (+)-**2**-H/(-)-**3**-H ($P2_1$) organize in different space groups, they exhibit close isostructural relationships as evident from inspection of their packing diagrams (Figs. 1A and B), unit cell parameters (ESI†), and X-ray diffraction patterns.

Both structures generate a complex network of N-H···O and O-H···O contacts that utilize each OH and NH hydrogen-bond donor. For (±)-**2**-H, this collection of contacts produces 12 unique hydrogen bonds [N/O···O, 2.6609(1)–3.045(1) Å; ∠ N/O-H···O 137(2)–176(2)°] for each racemic pair with tartaramide···tartaramide motifs described by both glide-plane and inversion symmetry relationships (Fig. 1A). Crystals of quasiracemate (+)-**2**-H/(-)-**3**-H achieve similar molecular alignment *via* 11 distinct N/O-H···O interactions per quasiracemic pair [N/O···O, 2.670(2)–3.347(2) Å; N/O-H···O 132(3)–174(3)°]. However, in this case, the glide and inversion relationships are only approximate owing to the difference in the OH/H substituents of the tartaramide and malamide components. While these crystal structures are markedly similar, the difference of an OH group (racemate) and a hydrogen atom (quasiracemate) results in one fewer hydrogen bond in the quasiracemate and several hydrogen bonds deviating from ideal contact geometries. This is most noticeable for the N2-H···O1 interaction, where the quasiracemate contact parameters (N···O, 3.347(2) Å; ∠ N-H···O, 150(3)°) are more decidedly non-ideal than those observed for the tartaramide racemate (2.908(1) Å and 176(2)°). This is likely because there are half as many N2-H···O1 interactions in the quasiracemate compared to (±)-**2**-H.

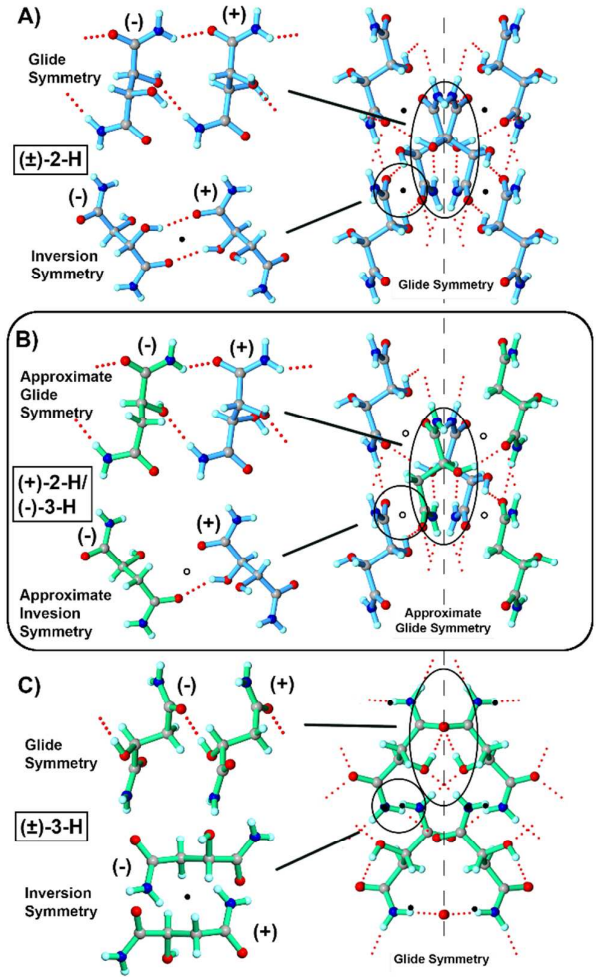

Fig. 1 Crystal structures of A) racemic tartaramide (±)-**2**-H B) quasiracemate (+)-**2**-H/(-)-**3**-H, and C) racemic malamide (±)-**3**-H showing hydrogen-bond contacts and packing motifs. An isostructural relationship exists between (±)-**2**-H and (+)-**2**-H/(-)-**3**-H where the quasiracemate components exhibit both approximate inversion and glide plane symmetry relationships. The dashed line represents glide and pseudo glide symmetry.

The crystal structure of racemate (±)-**3**-H is shown in Fig. 1C. While the malamide components organize with both inversion and glide symmetry relationships in space group $P2_1/c$, the observed molecular alignment is quite different than that of quasiracemate (+)-**2**-H/(-)-**3**-H and racemate (±)-**2**-H. This shift in crystal structure alignment can be directly attributed to the malamide molecular framework, where there is one less OH group than tartaramide. The outcome is that only 10 N-H···O and O-H···O contacts (2 less than (±)-**2**-H) form in the crystal. This supramolecular organization apparently offers better opportunities to maximize the efficiency of the available hydrogen bonds and other crystal packing features.

Secondary Amides. Given the success of producing quasiracemate (+)-**2**-H/(-)-**3**-H, we anticipated that extending our study to include a family of secondary amides would further highlight the utility of the tartaramide and malamide components as viable building-blocks for quasiracemate formation. The methyl and butyl amides were prepared using

modified literature procedures.[20-21] Crystal growth and subsequent crystallographic assessment of these materials clearly show pairs of the tartaramide and malamide derivatives; however, the molecular alignment lacks any noticeable near-inversion relationships.

The set of methyl amide crystal structures shown in Fig. 2 offers an important glimpse into the structural features of these new crystalline systems. The addition of methyl groups to the **2**-H and **3**-H molecular frameworks not only alters the molecular structure of the tartaramide and malamide components, but also the overall crystal structure landscapes. For example, molecules of (±)-**3**-Me possess 3 donor groups (Fig. 2A) that produce 6 N/O-H···O interactions per racemic pair. This is four fewer interactions compared to those observed in the structure of (±)-**3**-H (six fewer interactions when comparing the structure of (±)-**3**-Me to (±)-**2**-H). Similar to racemates (±)-**2**-H and (±)-**3**-H, molecules of (±)-**3**-Me organize in space group $P2_1/c$ with the N/O-H···O hydrogen-bonded motifs propagating in the *bc*-plane *via* glide-symmetry related components (Fig. 2A). This set of non-bonded contacts produces a 2D molecular sheet that further aligns with adjacent motifs using only van der Waals surfaces (*i.e.,* there are no hydrogen bonds between sheets). Regardless of the additional OH group present in quasiracemate (+)-**2**-Me/(-)-**3**-Me, the hydrogen-bond network and molecular organization of these 2D sheets are nearly indistinguishable to that observed in the structure of (±)-**3**-Me (Figs. 2A and 2B). Even so, a significant difference between these structures arises from the alignment of the adjacent molecular sheets. For (±)-**3**-Me, the neighboring 2D sheets arrange with inversion symmetry and in the crystal structure of quasiracemate (+)-**2**-Me/(-)-**3**-Me these motifs produce translationally related stacks in space group *P*1. As such, the crystal structure of the quasiracemate lacks centrosymmetrically related patterns likely due to the weak cohesive interactions between layers. Though the molecular structure of (±)-**2**-Me is similar to the quasiracemate and malamide, the organization of these building blocks is quite different (Fig. 2C). The additional OH group that accompanies tartaramide produces an extra O-H···O contact (8 total N/O-H···O contacts per racemic pair), producing supramolecular patterns in space group *Pccn* that are distinct from those observed for the structures of (+)-**2**-Me/(-)-**3**-Me and (±)-**3**-Me.

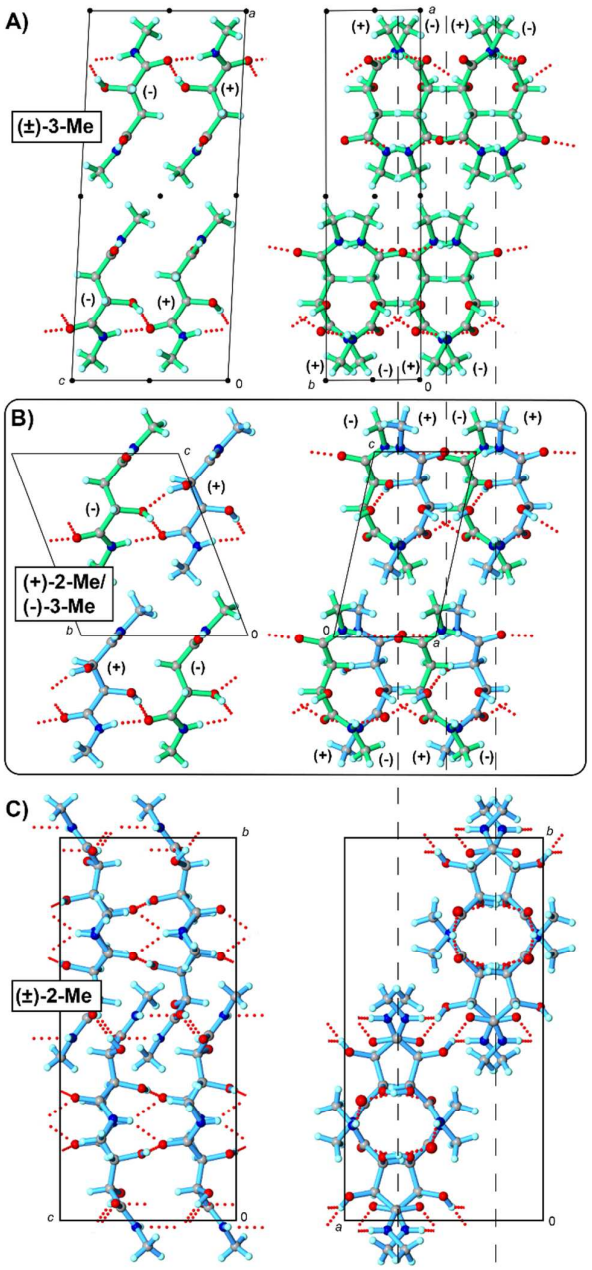

Fig. 2 Crystal structures of A) racemic malamide (±)-**3**-Me B) quasiracemate (+)-**2**-Me/(-)-**3**-Me, and C) racemic malamide (±)-**2**-Me showing hydrogen-bond contacts and packing motifs. An isostructural relationship exists between (±)-**3**-Me and (+)-**2**-Me/(-)-**3**-Me where the quasiracemate components exhibit only approximate glide plane symmetry relationships. Dashed lines represent glide and pseudo glide symmetry.

Inspection of the crystal densities [(+)-**2**-Me/(-)-**3**-Me, 1.392 g mL^{-1}; (±)-**3**-Me, 1.298 g mL^{-1}] and packing coefficients (C_k = 68.8 and 65.8%)[22] of these systems offers some initial insight to the structural consequence of these layered motifs. While the crystal density of the quasiracemate is considerably larger than the racemic counterpart, replacing the molecular weight of (±)-**3**-Me with that defined by the quasiracemate gives ρ = 1.3628 g mL^{-1} and C_k = 67.3%. These indicators of packing efficiency are only slightly less than those determined for (+)-**2**-Me/(-)-**3**-

Me. The consequence of similar crystal packing motifs and efficiencies seems clear - in the absence of strong directional contacts positioned at the interface of the molecular sheets, no obvious structural benefit exists to align these motifs with either inversion or translational symmetry.

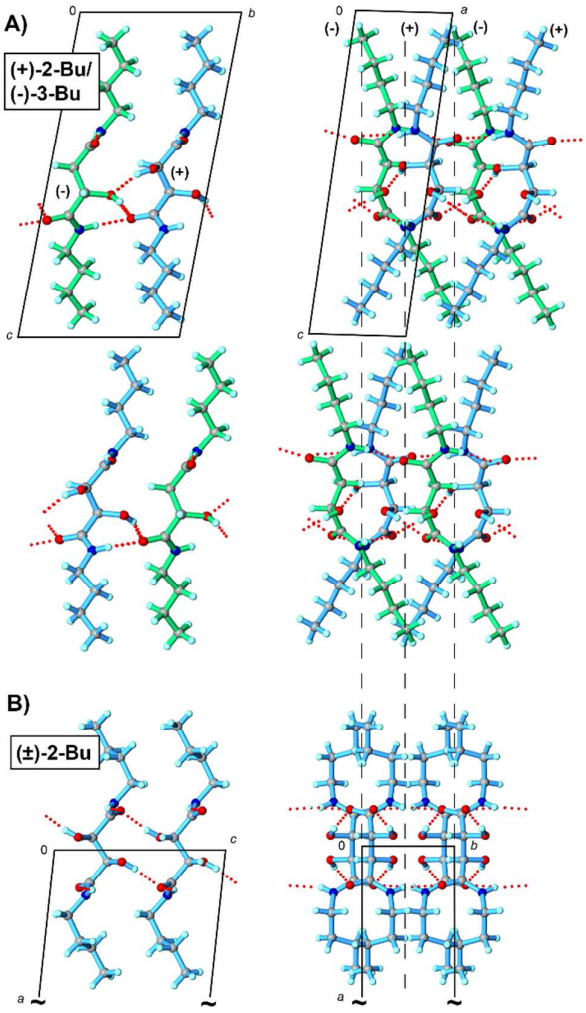

Fig. 3 Crystal structure of A) quasiracemate (+)-**2**-Bu/(-)-**3**-Bu and B) tartaramide (±)-**2**-Bu showing hydrogen bond contacts, packing motifs, and glide plane (or near glide plane) relationships between tartaramide and malamide components. Dashed lines represent glide and pseudo glide symmetry.

Additional evidence for the crystal packing features observed in (+)-**2**-Me/(-)-**3**-Me can be found in the structure of the butyl quasiracemate [(+)-**2**-Bu/(-)-**3**-Bu] (Fig. 3). Quasiracemates (+)-**2**-Me/(-)-**3**-Me and (+)-**2**-Bu/(-)-**3**-Bu are isostructural (*P*1) with nearly identical packing motifs and hydrogen-bond patterns. Each structure depicts translationally related molecular stacks with no approximate inversion symmetry. As shown in Fig. 3A, the added steric bulk of the butyl groups increases the distance between the core tartaramide/malamide components and is most pronounced along the *c*-axis. The crystal structure of (±)-**3**-Bu is quite distinct from the butyl quasiracemate, where the pendent butyl groups take on noticeably different conformations with molecules organized in *C*2/*c*.

Hirshfeld Surface Analysis. Hirshfeld surface fingerprint plots[23,24] were generated for each structure (Figs. 4 and S1). By plotting the internal (d_i) and external (d_e) distances from each nuclei to the Hirshfeld surface, the result is a 2D diagram highly sensitive to the immediate environment of the molecule. Visual inspection of the overall pattern of these diagrams offers important insight to the structural similarities and variations of these systems. For example, as anticipated, each structure shows sharp spikes located at the bottom left of the diagrams related to O···H contacts. Another area of particular interest is the diffuse region located between the spikes indicating close H···H contacts. For the structures with close isostructural relationships, these fingerprint plots are nearly indistinguishable. As an example, Fig. 4 shows the plots corresponding to the family of structures formed from the **2**-H and **3**-H components. The fingerprint plot signatures for (+)-**2**-H/(-)-**3**-H and (±)-**2**-H are almost interchangeable owing to the close packing features of each structure. This fingerprint plot similarity can also be seen with the (+)-**2**-Me/(-)-**3**-Me and (±)-**3**-Me structures (Fig. S1). The sensitivity and utility of this diagnostic tool becomes apparent when comparing systems with comparatively small [(+)-**2**-H/(-)-**3**-H and (±)-**3**-H] or large [(+)-**2**-Bu/(-)-**3**-Bu and (±)-**2**-Bu] crystal structural variations. In each case, these differences are readily distinguishable and offer visual evidence of the structural variation of these systems.

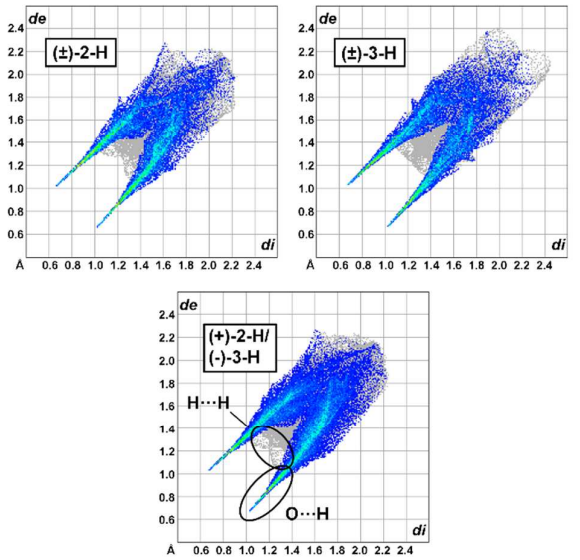

Fig. 4 Hirshfeld fingerprint plots for (±)-**2**-H, (±)-**3**-H, and (+)-**2**-H/(-)-**3**-H highlighting H···H and O···H contacts.

Glide-Plane Symmetry. A highlight of this study relates to the importance of glide symmetry to crystal packing of these tartaramide/malamide systems. Each of the examined crystal structures contain molecules organized by glide symmetry (or approximate glide symmetry). This symmetry element present in the racemic entries is also accompanied by inversion and/or two-fold rotation (2_1) symmetry elements to produce space groups $P2_1/c$ [(±)-**2**-H, (±)-**3**-H, and (±)-**3**-Me], *Pccn* [(±)-**2**-Me],

or *C*2/*c* [(±)-**3**-Bu]. Quasiracemate (+)-**2**-H/(-)-**3**-H contains both approximate inversion and glide symmetry, while those constructed from (+)-**2**-Me/(-)-**3**-Me and (+)-**2**-Bu/(-)-**3**-Bu show only translation and near glide-plane relationships.

For quasiracemate (+)-**2**-H/(-)-**3**-H, the components assemble *via* an intricate 3D hydrogen-bonded network and display approximate *b* glide symmetry perpendicular to the *c*-axis (Fig. 1). The pseudo mirror and *c*/2 translation closely relate the (+)-**2**-H and (-)-**3**-H quasienantiomers with the greatest deviation related to the OH and H groups. The molecular centroids of these tartaramide and malamide components are spaced at 0.4891*c* and 0.5109*c* (0.5*c* is needed for true glide symmetry), that when combined with a 2_1 symmetry operator gives packing motifs that mimic space group $P2_1/c$. Because the methyl amide quasiracemate, (+)-**2**-Me/(-)-**3**-Me, only contains two N-H groups per molecule, fewer opportunities exist for generating strong intermolecular contacts. The result is that the quasienantiomers organize in 2D molecular sheets *via* N-H···O contacts that propagate in the *ab* plane (Fig. 3). Unlike the structure of (±)-**3**-Me where the adjacent molecular sheets organize with near inversion symmetry, the molecular sheets observed in (+)-**2**-Me/(-)-**3**-Me promote stacking with only translationally related neighbors. In the absence of near inversion relationships, the dominant symmetry element that describes the alignment of the (+)-**2**-Me and (-)-**3**-Me components is pseudo *b* glide-plane symmetry perpendicular to the *a*-axis. The molecular centroids are spaced at 0.4976*b* and 0.5023*b* along the *c*-axis and indicate a slightly closer glide relationship than that observed in quasiracemate (+)-**2**-H/(-)-**3**-H. In the absence of additional symmetry, this motif approximates space group *Pb*11.

The structure of (+)-**2**-Bu/(-)-**3**-Bu offers an interesting addition to this study. Despite the obvious structural effect of attaching spatially larger butyl groups to the tartaramide/malamide framework, the organization of quasiracemate (+)-**2**-Bu/(-)-**3**-Bu components closely mimics that seen in the structure of (+)-**2**-Me/(-)-**3**-Me (Fig. 4). These structural similarities include supramolecular alignment, hydrogen-bond contacts, space group approximation (*Pb*11), and the lack of near inversion related motifs. Like all crystalline materials, quasiracemic systems do not require symmetry operations beyond translation; even so, the use of near-symmetry relationships can offer considerable benefit for close fitting of molecules. It has been estimated that roughly 92% of all known racemates crystallize in centrosymmetric space groups.[25-26] The other 8% of the entries organize the racemic pairs in non-centrosymmetric space groups using only rotational, screw-axis, and translation symmetry (Sohncke space groups). Since these materials are commonly referred to as kryptoracemates[27-28], it seems appropriate that this term lend itself to *kryptoquasiracemates* to describe quasiracemates such as (+)-**2**-Me/(-)-**3**-Me and (+)-**2**-Bu/(-)-**3**-Bu.

Lattice Energy Calculations

Several approaches using computational modelling were pursued to further probe the structural preferences observed for this family of tartaramide/malamide structures. The initial strategy involved geometry optimization of the observed crystal structures using quantum chemical simulations (DFT-D, using the PBE function[29] with the GD3BJ dispersion correction[30]) to compare stabilities of the crystal structures, as well as single-molecule calculations to allow decomposition of the total energies. In particular, we calculated four quantities for each structure: the lattice energy (E_{latt}, total crystal energy minus the intermolecular energy of the lowest energy isolated molecular geometry); intermolecular energy (E_{int}, total crystal energy minus the intramolecular energies of the molecules at their in-crystal geometries); intramolecular strain energy (E_{str}, the intramolecular energy at in-crystal molecular geometry relative to the nearest isolated-molecule conformer) and conformational energy (E_{conf}, the intramolecular energy at in-crystal molecular geometries relative to the lowest energy isolated molecular geometry). Full details of the computational methods are presented in the ESI†. Outcomes from these calculations were normalized by reporting energies for racemic or quasiracemic pairs of molecules.

As anticipated, the intramolecular energies for the **2**-H/**3**-H systems are quite similar owing to the isostructural nature of the (±)-**2**-H and (+)-**2**-H/(-)-**3**-H crystal structures (Table 1). The overall magnitudes of the intramolecular strain (E_{str}) and conformational energies (E_{conf}) are high compared to what is typically seen in small molecule crystal structures[31], indicating significant distortion of the molecular geometries due to intermolecular interactions; this likely arises from the optimization of intermolecular hydrogen-bond geometries, which is consistent with the slightly lower E_{str} for the less extensively hydrogen-bonded malamide compared to tartaramide.

The calculated lattice (E_{latt}) and intermolecular (E_{int}) interaction energies for these structures are also similar. The calculated intermolecular energy favors the racemate by 13.23 kJ mol^{-1} over the quasiracemate and is consistent with the loss of stabilization due to removing one O-H···O contact from each racemic tartaramide molecular pair. While the imposed OH/H structural difference of the tartaramide and malamide components seems significant when considering its potential effects to molecular alignment, the ~3% difference in interaction energies is comparatively small and offers important insight to why these systems adopt close isostructural relationships. Given the large number of N/O-H···O contacts for these systems (12 interactions for (±)-**2**-H and 11 for (+)-**2**-H/(-)-**3**-H per molecular pair), the energetic loss from removing one O-H···O interaction is not sufficient to force the molecules to adopt a different arrangement in the quasiracemate structure.

Table 1. DFT-D calculations for tartaramide(**2**)/malamide(**3**) systems (kJ mol^{-1})*

	Intermolecular Interactions (E_{int})	Molecular Strain (E_{str})**	Conformational Energy (E_{conf})**	Lattice Energy (E_{latt})***
(±)-**2**-H	-441.56	+24.57	+24.57	-392.43
(+)-**2**-H/ (-)-**3**-H	-428.33	+25.28, (+)-**2**-H +19.23, (-)-**3**-H	+25.41, (+)-**2**-H +19.23, (-)-**3**-H	-383.82
(±)-**2**-Me	-403.61	+28.85	+29.28	-345.04

(±)-**3**-Me	-372.93	+16.07	+20.17	-332.58
(+)-**2**-Me/ (-)-**3**-Me	-391.41	+31.78, (+)-**2**-Me +21.07, (-)-**3**-Me	+31.78, (+)-**2**-Me +21.07, (-)-**3**-Me	-338.55
(±)-**2**-Bu	-445.51	+38.14	+40.61	-364.29
(+)-**2**-Bu/ (-)-**3**-Bu	-455.71	+47.30, (+)-**2**-Bu +35.83, (-)-**3**-Bu	+47.30, (+)-**2**-Bu +35.83, (-)-**2**-Bu	-372.59

* All intermolecular and lattice energies are given per pair of molecules for the quasiracemates and, for comparison, per racemic pair of molecules.
** Molecular strain energies were calculated per single molecule and as the difference between the energy of the molecule in its in-crystal geometry (after DFT-D optimization) and the energy of the molecule after optimization to the nearest gas-phase minimum (not necessarily the most stable gas phase conformer). Conformational energies were calculated by comparing the in-crystal molecule with the lowest energy conformer for each molecule (from the optimized molecules taken from all crystal structures).
*** Lattice energies are taken as the energies of the crystals relative to the gas phase state of the constituents. These are calculated as the sum of the intermolecular energy and the molecular energy in the crystal relative to the most stable gas phase conformer. In the absence of exhaustive conformational searches, the gas phase molecular energies are taken as the lowest energy resulting from optimization of the molecules taken from all known crystal structures (*e.g.* for **2**-H molecules, the lower energy of the tartaramide molecules optimized starting from the (±)-**2**-H and the (+)-**2**-H/(-)-**3**-H structures. In this case, the two tartaramide molecules optimized to conformers with similar energies).

We also compared the DFT-D calculations for (±)-**2**-H and (+)-**2**-H/(-)-**3**-H to results obtained using the molecular cluster approach employed by *CrystalExplorer*[32] (B3LYP/6-31G(d,p)) (ESI†). These two methods produce very similar results with ΔE_{int} = 13.2 (DFT-D) and 14.8 (direct summation of interactions, ref. 28) kJ mol^{-1}. Both methods indicate slightly increased lattice stabilization achieved by the (±)-**2**-H structure as compared to quasiracemate (+)-**2**-H/(-)-**3**-H. These computational results were further supported experimentally by use of differential scanning calorimetry (DSC). Outcomes from these DSC traces showed the expected trends in crystal lattice stabilization [(±)-**2**-H (mp = 221.98 °C, H_f = -78.13 kJ mol^{-1}); (+)-**2**-H/(-)-**3**-H (mp = 178.24 °C, H_f = -72.46 kJ mol^{-1}); (±)-**3**-H (mp = 162.86 °C, H_f = -68.95 kJ mol^{-1}).

While crystallographic, computational modelling, and DSC studies of the **2**-H/**3**-H system support the idea that cocrystallization of pairs of quasienantiomers results from their complementary topologies, until now all reported quasiracemate structures mimic centrosymmetric alignment. The structures of (+)-**2**-Me/(-)-**3**-Me and (+)-**2**-Bu/(-)-**3**-Bu offer important departures from the extant database of quasiracemic structural preferences where the quasienantiomeric components are aligned only by near-glide symmetry.

DFT-D calculations performed on the family of **2**-Me/**3**-Me structures show that the intermolecular energies and lattice energies correlate with the extent of hydrogen bonding. Thus, the stability of the quasiracemate structure is positioned between the two racemates (Table 1). The calculations also indicate that the conformers of both methyl malamide and tartramide are more strained in the quasiracemate (+)-**2**-Me/(-)-**3**-Me than either racemate.

To further probe these structures and understand why they lack approximate inversion symmetry, we then considered OH/H group replacements to generate hypothetical quasiracemates with approximate inversion symmetry from the observed racemates. Converting the structure (±)-**2**-Me (*Pccn*) to the hypothetical quasiracemate required replacing one of the OH groups with an H atom. Since the tartaramide moiety contains two hydroxyl groups, this substitution process resulted in two distinct hypothetical models whose DFT-D lattice energies are ΔE_{latt} = +29.62 and +9.07 kJ mol^{-1} as compared to the corresponding experimentally derived quasiracemate. Similarly, we created hypothetical quasiracemates from the observed methyl malamide racemate (±)-**3**-Me by replacing the H atom of one racemic pair with an OH group to construct a new hypothetical quasiracemate. While only one OH/H substitution is necessary in this case, the newly placed OH group has two possible orientations that form intermolecular hydrogen bond contacts (*i.e.,* O-H···O=C and O-H···$O_{hydroxyl}$) (Fig. 5). However, the geometries of the newly introduced hydrogen bonds are strained and the resulting structures have calculated lattice energies ΔE_{latt} = +20.02 (Fig. 5, top) and +4.13 kJ mol^{-1} (Fig. 5, bottom)above the observed (+)-**2**-Me/(-)-**3**-Me structure. Thus, all of the four hypothetical quasiracemates built from the structures of the parent racemates are less stable than observed crystal structure.

Construction and DFT-D geometry optimization of hypothetical quasiracemates for the butyl amides [(±)-**2**-Bu (C2/c) and (+)-**2**-Bu/(-)-**3**-Bu] gave an even clearer picture when compared to the experimental quasiracemate. The hypothetical butyl quasiracemate structures created from the observed structure of (±)-**2**-Bu gave calculated lattice energies of +22.90 and +23.19 kJ mol^{-1} above the experimental quasiracemate.

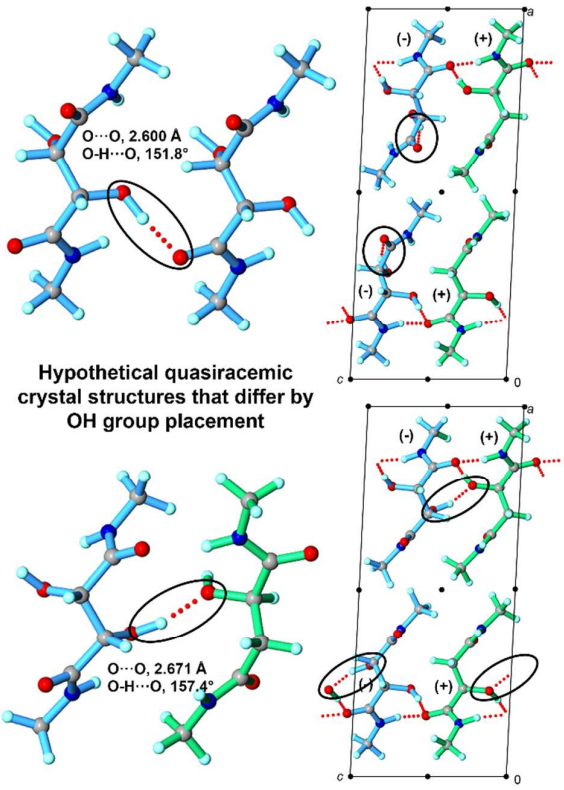

Fig. 5 Hypothetical quasiracemic crystal structures generated from (±)-**3**-Me showing the two possible OH orientations, newly imposed O-H···O contacts, and crystal packing patterns. The lattice energies relative to the observed quasiracemate are 20.02 (top) and 4.13 (bottom) kJ mol^{-1}

The main outcome from these computational experiments based on replacing one component of the racemate (tartaramide or malamide) to generate a simulated quasiracemate is that this decreases the lattice stabilization as compared to the observed quasiracemic crystal structures. In other words, the near inversion symmetry imposed on the hypothetical methyl and butyl quasiracemic structures does not provide models that are of any energetic benefit compared to pure translationally related stacks of quasiracemic components.

Conclusion

In conclusion, quasiracemates offer an effective approach to molecular assembly that build on the structural features of true racemic materials. Until now, the prevailing thought was that quasiracemic materials exist because of the complementarity of quasienantiomeric molecular shapes that, when crystallized, give way to thermodynamically controlled close packing achieved by inversion related motifs. The tartaramide/malamide system is all the more remarkable given the significant structural variation of the OH and H groups. For (±)-**2**-H and (+)-**2**-H/(-)-**3**-H, these systems are isostructural and surprisingly only differ in intermolecular interaction energies by 3% despite the additional O-H···O contact with the racemate. Quasiracemates (+)-**2**-Me/(-)-**3**-Me and (+)-**2**-Bu/(-)-**3**-Bu crystallize in space group *Pb*11 and only organize with approximate glide-plane symmetry. Calculations based on the observed crystal structures and simulated quasiracemic models offer an effective computational approach for assessing these tartaramide/malamide systems. In each case, outcomes from these studies show that the experimental quasiracemates achieve crystal packing stabilities that surpass those derived from the racemic tartaramide and malamide structures.

Acknowledgements

This work was generously supported by the National Science Foundation (DMR1505717 and CHE0722547) and Whitworth University. We also acknowledge the ARCHER UK National Supercomputing Service which was accessed via the UK's HPC Materials Chemistry Consortium, which is funded by the EPSRC (EP/L000202). We thank Prof. A. L. Rheingold for key crystallographic contributions and Profs. C. P. Brock and B. M. Foxman for helpful discussions.

Conflicts of interest

There are no conflicts of interest to declare.

Notes and references

1 L. Pasteur, *Ann. Chim. Phys.*, 1853, **17**, 438-483.
2 L. Pasteur, *Compt. Rend. Acad. Sci.*, 1853, **19**, 162-166.
3 L. Pasteur, *Ann. Chim. Phys.*, 1850, **28**, 56-99.
4 L. Pasteur, *Ann. Chim. Phys.*, 1848, **24**, 442-459.
5 J. Gawronski and K. Gawronska, *Tartaric and Malic Acids in Synthesis: A Source Book of Building Blocks, Ligands, Auxiliaries, and Resolving Agents*, Wiley-Interscience: New York, 1999.
6 X. Ma, Q. Yan, M. G. Banwell and J. S. Ward, *Org. Lett.*, 2018, **20**, 142-145.
7 L. Zhang, C. Zhang, W. Zhang, Z. Cui, P. Fu, M. Liu, X. Pang and Q. Zhao, *ACS Omega*, 2018, **3**, 2463-2469.
8 Z. G. Brill, H. K. Grover and T. J. Maimone, *Science*, 2016, **352**, 1078-1082.
9 K. A. Wheeler, R. C. Grove, R. E. Davis and W. S. Kassel, *Angew. Chem., Int. Ed.*, 2008, **47**, 78-81.
10 A. J. Cruz-Cabeza, M. Lestari and Matteo Lusi, *Cryst. Growth Des.*, 2018, **18**, 855-863.
11 G. B. Kauffmanm and R. D. Myers, *J. Chem. Ed.,* 1975, **52**, 777-781.
12 A. Fredga, *Bull. Soc. Chim. Fr.*, 1973, **1**, 173-182.
13 G. Lautrette, B. Kauffmann, Y. Ferrand, C. Aube, N. Chandramouli, D. Dubreuil and I. Huc, *Angew. Chem., Int. Ed.*, 2013, **52**, 11517-11520.
14 M. D. Eddleston, M. Arhangelskis, T. Friščić and W. Jones, *Chem. Commun.*, 2012, **48**, 11340-11342.
15 C. Roth, D. Passerone and K.-H. Ernst, *Chem. Commun.*, 2010, **46**, 8645-8647.
16 R. Wartchow, *Z. Kristallogr.*, 1996, **211**, 329-330.
17 R. Kostyanovsky, E. Nikolaev, O. Kharybin, G. Kadorkina and V. Kostyanovsky, *Mendeleev Commun.*, 2003, **3**, 97-99.
18 C. B. Aakeröy, T. I. Cooke and M. Nieuwenhuyzen, *Supramol. Chem.*, 1996, **7**, 153-156.
19 C. R. Taylor and G. M. Day, *Cryst. Growth Des.*, 2018, **18**, 892-904.
20 P. F. Frankland and A. Slator, *J. Chem. Soc., Trans.*, 1903, **83**, 1349-1367.
21 B. A. Shainyan, M. V. Ustinov, V. K. Belśkii and L. O. Nindakova, *Russ. J. Org. Chem.*, 2002, **38**, 104-110.
22 The packing coefficient is defined as the ratio of the volume of the molecules in the unit cell to the volume of the unit cell, $C_k = V_{mol}/V_{cell}$: A. I. Kitaigorodsky, Molecular Crystals and Molecules, Academic Press, New York, 1973.
23 M. A. Spackman and D. Jayatilaka, *CrystEngComm*, 2009, **11**, 19-32.
24 M. A. Spackman and J. J. McKinnon, *CrystEngComm*, 2002, **4**, 378-392.
25 M. Hendi, P. Hooter, V. Lynch, R. E. Davis and K. A. Wheeler, *Cryst. Growth Des.,* 2004, **4**, 95-101.
26 B. Dalhus and C. H. Görbitz, *Acta Crystallogr., Sect. B: Struct. Sci.*, 2000, **B56**, 715-719.
27 R. Laubenstein, M.-D. Şerb, U. Englert, G. Raabe, T. Braun and B. Braun, *Chem. Commun.,* 2016*,* **52**, 1214-1217.
28 L. Fábián and C. P. Brock, *Acta Crystallogr., Sect. B: Struct. Sci.*, 2010, **B66**, 94-103.
29 J. P. Perdew, K. Burke and M. Ernzerhof, *Phys. Rev. Lett.,* 1996, **77**, 3865-3868.
30 S. Grimme, S. Ehrlich and L. Goerigk, *J. Comp. Chem.*, 2011, **32**, 1456-1465.
31 H. P. G. Thompson and G. M. Day, *Chem. Sci.*, 2014, **5**, 3173-3182.
32 S. P. Thomas, P. R. Spackman, D. Jayatilaka, M. A. Spackman, *J. Chem. Theory Comput.*, 2018, **14**, 1614-1623.

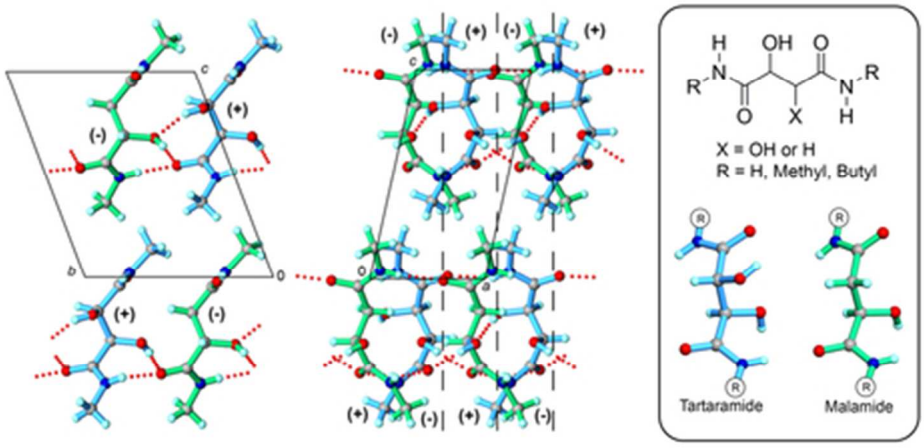

39x19mm (300 x 300 DPI)